Desalination and Water Treatment
www.deswater.com

doi: 10.1080/19443994.2015.1088478

57 (2016) 17011–17022
August

Taylor & Francis
Taylor & Francis Group

Adsorptive removal of methyl orange using enhanced cross-linked chitosan/bentonite composite

Lujie Zhang, Qian Liu, Pan Hu, Ruihua Huang*

College of Science, Northwest A & F University, Yangling, Shaanxi 712100, China, Tel. +86 029 87092226;
emails: 25475492@qq.com (L. Zhang), 1185898219@qq.com (Q. Liu), 1515325595@qq.com (P. Hu), hrh20022002@163.com (R. Huang)

Received 7 April 2015; Accepted 3 August 2015

ABSTRACT

In this study, the cross-linked chitosan/bentonite composite was treated further with concentrated HCl. The resultant composite was referred to as the enhanced cross-linked chitosan/bentonite (ECCS/BT) composite, which was characterized by X-ray diffraction, scanning electron microscopy, and Fourier transform infrared spectroscopy techniques. ECCS/BT composite was used as an adsorbent to remove an anionic dye, methyl orange (MO), from aqueous solutions by a batch method. Various conditions were evaluated, including acid treatment, the ratio of chitosan to bentonite, initial MO concentration, adsorbent dosage, solution pH, and contact time. The adsorption kinetics and equilibrium isotherms of MO by the ECCS/BT composite were studied using the pseudo-first-order and pseudo-second-order kinetic models as well as Freundlich and Langmuir isotherm models. The kinetic data followed the pseudo-second-order equation; the isotherm data were described by the Langmuir isotherm model and the maximum adsorption capacity (Q_{max}) was obtained at 136.8 mg/g at natural pH and 293 K.

Keywords: Enhanced cross-linked chitosan/bentonite composite; Methyl orange; Adsorption; Kinetics

1. Introduction

Many kinds of dyes are being used in many industries including textile, tannery, papermaking, electroplating, and food processing. Dyes usually have a synthetic origin and complex chemical structure which makes them very stable to light and oxidation and very difficult to biodegrade [1]. If these dyes are not treated before discharging into a water system, it would cause various environmental problems [2]. Several physical, chemical, and biological techniques have been employed to remove dyes from wastewaters, such as photochemical degradation, biological degradation, coagulation, chemical oxidation, and adsorption [3–8]. Among these methods, adsorption has been thought to be the most promising option for the removal of dyes from wastewaters. Of all the adsorbents, activated carbon is often used due to its porous nature and large surface area [9]. However, it is quite expensive and difficult to recover [10], thus, its broad application was restricted to some degree. This has prompted a search for cheap and efficient alternative materials, such as bagasse pith, wood, fly ash, rice husk, and clay.

*Corresponding author.

Bentonite (BT) is a kind of low-cost and abundant clay that is primarily composed of montmorillonite (Mt). However, natural bentonite only removes weak dyes from water due to the strong hydration of its inorganic exchangeable ions. Therefore, bentonite was modified with organic cations or by combination with some biomaterials, such as chitosan, chitin, and lignin. Chitosan (CS) is an alkaline deacetylated product of chitin, characterized by high hydrophilicity and large number of hydroxyl and amino groups, and is considered as an environmentally friendly material with minimal toxicity, biocompatibility, biodegradability, and great availability in nature [11]. Besides, chitosan can maintain good compatibility with clay minerals [12,13]. However, using pure chitosan as an adsorbent has several disadvantages, such as being costly and low stability in acidic media. To prevent the dissolution of chitosan in acidic media, cross-linking agents including epichlorohydrin, tripolyphosphate, and glutaraldehyde have been frequently employed to enhance the stability of chitosan. Cho et al. developed a composite adsorbent by entrapping cross-linked chitosan and nano-magnetite on heulandite surface to remove Cu(II) and As(V) from aqueous solution [14]. To decrease the cost of chitosan-based adsorbents, immobilizing chitosan on a low-cost material, like bentonite, sand, and montmorillonite, was an effective modification method. Pereira et al. prepared chitosan–montmorillonite beads by cross-linking with pentasodium tripolyphosphate, and investigated the adsorption of Cu(II) from aqueous solutions onto this biocomposite [15]. In our previous study, we reported the cross-linked chitosan/bentonite (CCS/BT) composite for the removal of methyl orange (MO). The cross-linked chitosan/bentonite (CCS/BT) composite showed a high adsorption capacity, and the maximum adsorption capacity of CCS/BT composite calculated by the Langmuir model was 224.8 mg/g [16]. However, the amount of chitosan in this composite was still great.

In the present study, in order to decrease the amount of chitosan, the cross-linked chitosan/bentonite composite with the ratio of chitosan to bentonite (2/5) would be treated with concentrated HCl for the activation of bentonite and the protonation of cross-linking chitosan. The enhanced cross-linked chitosan/bentonite composite (ECCS/BT) exhibited a relatively high adsorption capacity for MO. Surface morphology characterization and structural analysis of the ECCS/BT composite were done by scanning electronic microscopy (SEM), X-ray diffraction (XRD), and Fourier transform infrared spectroscopy (FTIR) techniques. The effects of adsorption conditions, such as contact time, solution pH, adsorbent dosage, and initial MO concentration, were investigated. In addition, the adsorption isotherms and kinetic behaviors of MO onto the ECCS/BT composite were studied in detail.

2. Materials and methods

2.1. Reagents

Chitosan was supplied by Sinopharm Group Chemical Reagent Limited Company (China) with a degree of deacetylation of 90% and average molecular weight of 10^5 g/mol. Bentonite powder with a particle size of 200 mesh was acquired from the chemical factory of Shentai, Xinyang, Henan, China. MO was supplied by Sigma chemical company, and was used as adsorbate in the tests. All other reagents used were analytical grade reagent. Deionized water was used for all aqueous solutions.

2.2. Preparation of ECCS/BT composite

CCS/BT composite in powder form was prepared according to our previous study [13]. The CCS/BT composite was treated with concentrated HCl for 60 min for the protonation of cross-linked chitosan and the activation of bentonite. The resultant composite was named as the ECCS/BT composite, washed with distilled water to neutral pH, dried at 60˚C in an oven, and ground. The ECCS/BT composite particles of 100-mesh size were obtained, and used for adsorption studies.

2.3. Measurement of MO

Stock solution (1,000 mg/L) of MO was prepared by dissolving 1 g of MO into 1,000 mL of deionized water. The stock solution was then diluted to give standard solutions of appropriate concentration. MO concentration measurements were carried out using a UV–vis spectrometer (Shanghai Precision & Scientific Instrument Co., Ltd, 754-N, China) at 464 nm. The pH value of dye solution was determined with the Leici acidity meter (Leici pHs-3c, Shanghai, China).

2.4. Characterization of ECCS/BT composite

Surface morphology images of the samples were observed by field emission scanning electronic microscope (FE-SEM) (Hitachi S4800). XRD profiles of the samples were performed using a Shimadzu XD3A diffractometer equipped with a monochromatic Cu Ka source operating at 40 kV and 30 mA. FTIR spectra were collected with a spectrometer (Shimadzu 4100)

using KBr pellets. The diffraction patterns were recorded from 3° to 55° with a scan rate of 0.02°/s. The zero point of charge (pH_{ZPC}) of the sample was measured by the solid addition method.

2.5. Adsorption of MO onto the ECCS/BT composite

Adsorption experiments were performed in conical flasks containing 50 mL of MO solution and required dosage of adsorbent at specified temperature. The flasks were shaken at 200 rpm. When the predefined contact time attained, the adsorbent was separated by filtration. The concentration of MO in the filtrate was measured. The adsorption capacity for MO at any time, t (q_t, mg/g), was calculated using the following equation:

$$q_t = \frac{(C_0 - C_t)V}{W} \quad (1)$$

where C_t (mg/L) is the dye concentration at any time t (min), C_0 (mg/L) is the initial MO concentration, W (g) is the adsorbent dosage, and V (L) is the volume of MO solution.

2.6. Adsorption isotherm models of MO

Adsorption isotherms of MO on ECCS/BT composite were determined at 293, 303, 313, and 323 K, respectively, with desired concentration, natural pH, and 180 min of contact time. Eq. (1) can be used to calculate the equilibrium capacity of MO on the ECCS/BT composite (q_e, mg/g), and the C_t in the equation can be changed to C_e (the equilibrium MO concentration in solution, mg/L). The Langmuir and Freundlich isotherm models were used to describe the linear forms about the adsorption of MO on the ECCS/BT composite.

2.7. Adsorption kinetics of MO

Adsorption kinetics of MO on the ECCS/BT composite was investigated by batch experiments at initial MO concentrations (50, 100, and 150 mg/L, respectively). Separate flasks were prepared for each time interval and only one flask was taken out for the desired time. In order to investigate the mechanism of adsorption, the pseudo-first-order and pseudo-second-order models have been used for the adsorption processes.

2.8. Desorption and regeneration studies

Desorption studies were also conducted in the batch mode. Similar to adsorption studies, 0.05 g of fresh adsorbent was added to 50 mL of MO solution (100 mg/L). After 24 h at room temperature, the saturated MO-loaded adsorbent was collected by filtration and washed with distilled water in order to remove the unadsorbed traces of MO. Then, the adsorbent was agitated with 50 mL of 0.1, 0.3, and 0.5 mol/L HCl or 0.1, 0.3, and 0.5 mol/L NaOH solutions for 24 h, followed by adsorbent separation from the eluent, and washed with distilled water for several times to remove excessive acidity/alkalinity. Finally, the adsorbent was dried at 60°C for 12 h. To test the reusability of the adsorbent, the adsorbent was applied in the adsorption of MO (100 mg/L). The regeneration rate (RR) was calculated according to the following equation:

$$RR = \frac{(R_{fre} - R_{reg})}{R_{fre}} \times 100\% \quad (2)$$

where the values for R_{fre} and R_{reg} are the removals toward MO using the fresh adsorbent and regenerative one, respectively.

3. Results and discussion

3.1. Characterization of the ECCS/BT composite

Fig. 1 shows the XRD patterns of CS, the protonated cross-linked chitosan, BT, the BT treated with concentrated HCl, and the ECCS/BT composite. The XRD pattern of CS (Fig. 1(a)) showed the characteristic crystalline peaks at 11.2° and 22.4° [17]. However, the natural crystal peak at 11.2° disappeared and the peak at 22.4° weakened obviously in the protonated cross-linked chitosan, as shown in Fig. 1(b), indicating that the crystallinity degree of chitosan was destroyed due to the cross-linking reaction and the protonation of $-NH_2$ groups. The XRD pattern of BT (Fig. 1(c)) exhibited a typical reflection of montmorillonite at 6.56°. However, after BT was treated with concentrated HCl, the peak at 28° assigned to the characteristic peak of feldspar disappeared, and the typical reflection of montmorillonite was shifted from 6.56° to 5.96°, suggesting an increase in basal spacing, as shown in Fig. 1(d). For the ECCS/BT composite (Fig. 1(e)), this peak attributed to a typical reflection of montmorillonite at 5.96° was shifted to a smaller angle as compared with the bentonite treated with concentrated HCl, indicating the intercalation of chitosan into bentonite.

The surface images of BT, the BT treated with concentrated HCl, and the ECCS/BT composite were observed by FE-SEM. The results are shown in Fig. 2.

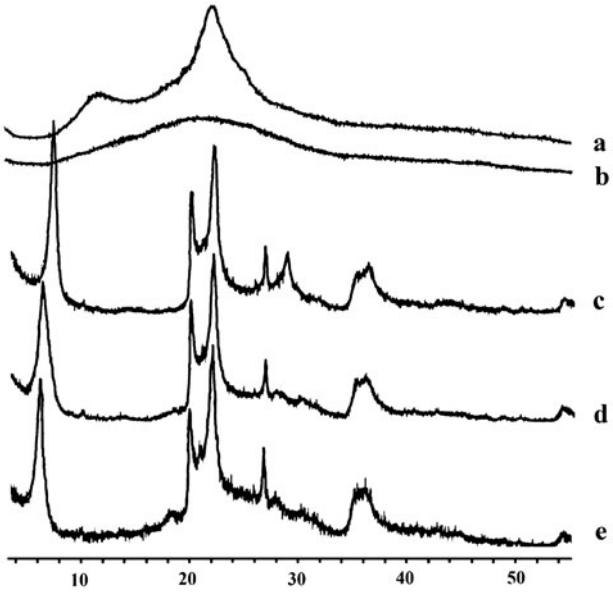

Fig. 1. XRD patterns for various materials: (a) chitosan, (b) protonated cross-linked chitosan, (c) bentonite, (d) acid-activated bentonite, and (e) enhanced cross-linked chitosan/bentonite composite.

As shown in Fig. 2(a), the original BT was characterized by a drusy texture, partially developed crystalline laminar and conglomerates of compact crystals. The surface images of BT treated with concentrated HCl and ECCS/BT composite were different from that of original bentonite. After bentonite was activated by concentrated HCl, the crystalline laminar of bentonite cracked open, and its surface structure became loose, as shown in Fig. 2(b). However, when bentonite was covered with cross-linked chitosan molecules and treated with concentrated HCl, the crystals of bentonite could not be seen clearly, and the structure became compact as compared with the acid-activated bentonite, which confirmed the combination of bentonite with chitosan.

The FTIR spectra of the ECCS/BT composite samples before and after MO adsorption are illustrated in Fig. 3. The peak at 1,643 cm^{-1} in the ECCS/BT composite was assigned to the N–H bending vibration. The vibrations of silica group comprising of Si–O–Si symmetric and asymmetric stretches, Si–O–Si bend, and silanol Si–O stretches were found between 467 and 1,039 cm^{-1}, which were attributed to the characteristic peaks of bentonite. After the ECCS/BT

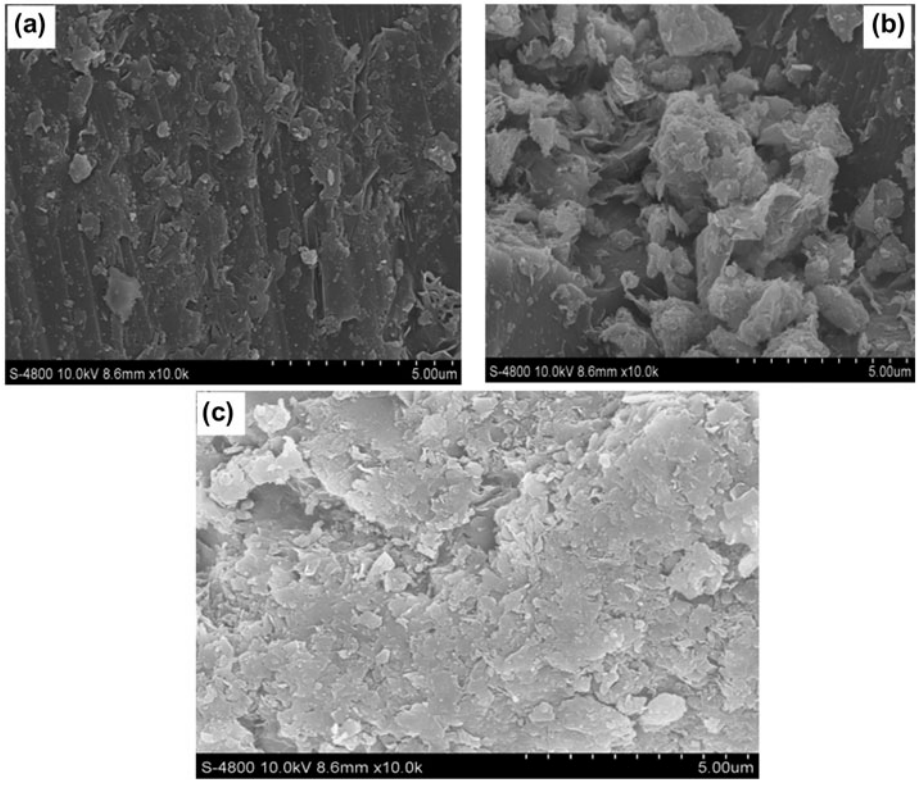

Fig. 2. SEM images for bentonite (a), acid-activated bentonite, and enhanced cross-linked chitosan/bentonite composite (c).

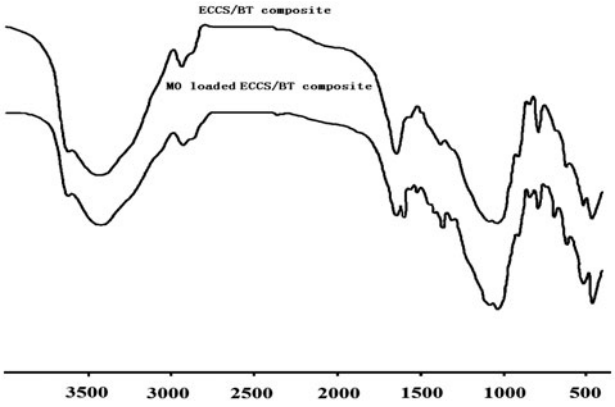

Fig. 3. FTIR spectra of ECCS/BT composite and MO-loaded ECCS/BT composite.

composite was loaded by MO molecules, this peak at 1,643 cm^{-1} clearly weakened, suggesting the involvement of amine groups in the adsorption of MO. Meanwhile, the intensity of the peak at 793 cm^{-1} attributed to the symmetric stretching vibration of Si–O–Si was weakened and other characteristic peaks of bentonite were shifted slightly, suggesting that MO adsorption also occurred on the surface of bentonite. Besides, some new peaks were observed in the FTIR spectrum of the MO-loaded ECCS/BT composite. The peak at 1,603 cm^{-1} was assigned to the characteristic peak of aromatic ring [18,19]. The peak at 1,368 cm^{-1} was attributed to $-CH_3$ bending vibration [18,19]. These observations confirmed the presence of MO molecules.

The determination of the pH_{ZPC} of the sample was carried out using a procedure as described previously by El Qada et al. [20]: 50 ml of 0.1 mo/L NaCl solutions were placed in 150-mL conical flasks. Initial pH of 0.1 mo/L NaCl solutions (pH_i) was adjusted from pH 2 to 11 by adding either 0.1 mol/L HCl or 0.1 mol/L NaOH solution. Adsorbent dosage (0.05 g) was added to 50 mL of 0.1 mol/L NaCl solution and stirred for 120 min and final pH (pH_f) of solution was measured. The difference between the initial and final pH ($pH_f - pH_i$) was plotted against the initial pH (pH_i) and the point where $pH_f - pH_i = 0$ was thought to be the zero point of charge (pH_{ZPC}) of adsorbent (Fig. 4). The pHpzc of zirconium-immobilized bentonite was found to be 6.5 or so.

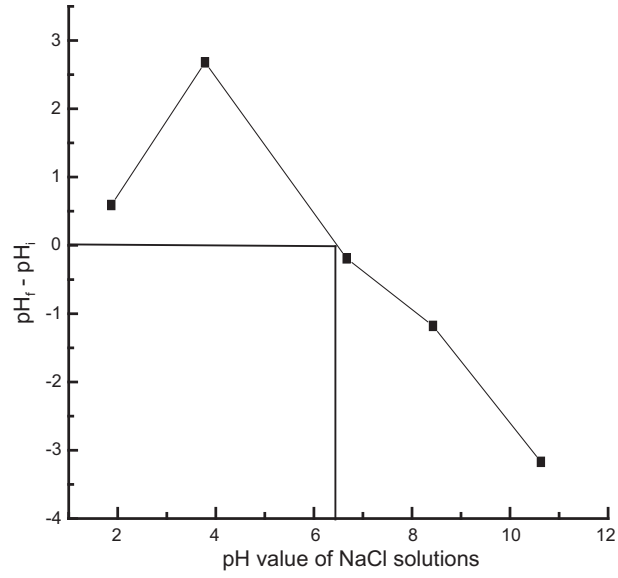

Fig. 4. Determination of pH_{ZPC} of ECCS/BT composite.

3.2. Effect of acid treatment on MO adsorption

To improve the adsorption for MO by the CCS/BT composite, the CCS/BT composite was treated with acid for the activation of BT and the protonation of $-NH_2$ groups in CS. HCl and HNO_3 solutions with various concentrations were applied in the treatment of the CCS/BT composite. The results are shown in Fig. 5. The CCS/BT composite treated with acid allowed higher removal than the CCS/BT composite. The removal increased gradually with an increase in HNO_3 concentration until it was 6 mol/L, and then it reduced slightly. However, the removal increased with an increase in HCl concentration, and the CCS/BT composite treated with concentrated HCl showed the maximum removal toward MO. This high removal

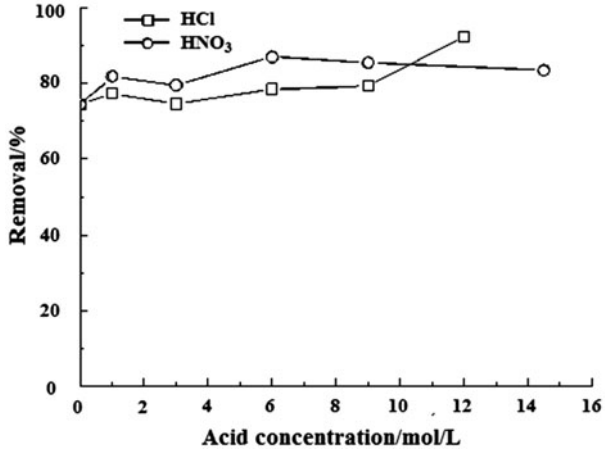

Fig. 5. Effect of acid treatment on MO adsorption.

may be attributed to the activation of BT and the protonation of $-NH_2$ groups in CS. For the activation of BT, acid treatment was helpful to increase the basal spacing of bentonite and dredge the inner passage in bentonite, as shown in Fig. 1(d). An increase in basal spacing and the dredged inner passage can provide a better adsorption of MO onto this composite. For the protonation of $-NH_2$ groups in chitosan, Viswanathan et al. prepared protonated cross-linked chitosan beads for fluoride adsorption. After the cross-linked chitosan beads were treated with concentrated HCl for the protonation of beads, the protonated cross-linked chitosan beads has shown high removal for fluoride due to strong electrostatic interaction between positively charged surface and negatively charged fluoride ions [21]. In this study, the CCS/BT composite was treated with concentrated HCl for the protonation of chitosan; an increase in electropositivity would facilitate the adsorption of anion dye (MO). Therefore, the concentrated HCl was chosen for the treatment of the CCS/BT composite.

3.3. Effect of the ratio of chitosan to bentonite on MO adsorption

Fig. 6 shows the effect of the ratio of chitosan to bentonite in the ECCS/BT composite on MO adsorption. At the given adsorption conditions, T (293 K), pH (unadjusted), contact time (60 min), MO concentration (100 mg/L), and adsorbent dosage (1 g/L), the ECCS/BT composite has shown a diametrically high removal as compared with both the protonated cross-linked chitosan and acid-activated bentonite as expected. This high removal may be due to the activation of bentonite and the protonation of $-NH_2$ groups in chitosan. However, decreasing this ratio weakened the adsorption of MO, suggesting that increasing content of bentonite in the ECCS/BT composite was adverse to the adsorption of MO onto the ECCS/BT composite. In this study, the ratio of chitosan to bentonite in adsorbent (2/5) was adopted because the ECCS/BT composite prepared at this ratio exhibited relatively high removal.

3.4. Effect of pH of MO solution on MO adsorption

The initial pH value of dye solution is recognized as an important operational parameter which can significantly affect the adsorption mechanisms between dye molecules and the adsorbent. The adsorption conditions are listed as follows: T (293 K), contact time (60 min), MO concentration (50 mg/L), and adsorbent dosage (1 g/L), the effect of pH on MO adsorption onto the ECCS/BT composite was studied with an initial pH of 1, 3, 5, 7, 8, 9, and 11. The pH_{ZPC} of the ECCS/BT composite was obtained at pH 6.5 or so (Fig. 4). The surface of the adsorbent will be negatively charged above pH_{ZPC} and positively charged below pH_{ZPC}. Our results (Fig. 7) revealed that the maximum removal occurred at pH 3. At pH (>9) and pH (<3), the removal decreased drastically. Its pK_a value in water is close to 3.4 [22]. MO has two chemical structures, whose chromophores are anthraquinone or azo bond depending on the pH of the solution [23], as can be expressed as follows:

At pH <3 (<pH_{ZPC}), the MO existed in left pattern, the number of negatively charged sites in MO decreased, while the surface of the adsorbent was

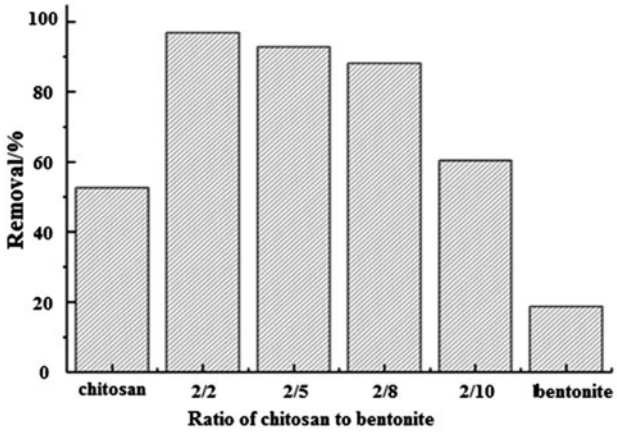

Fig. 6. Effect of the ratio of chiosan to bentonite on MO adsorption.

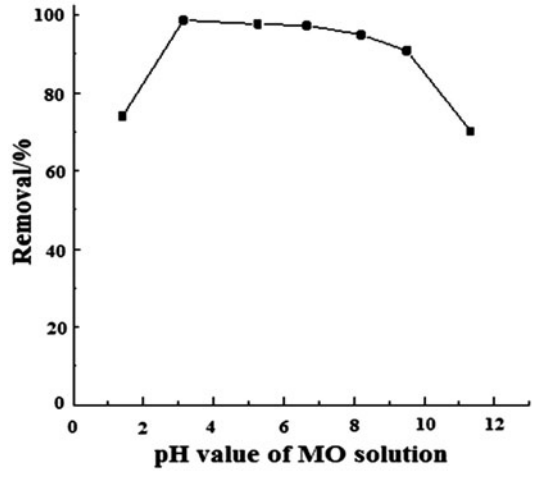

Fig. 7. Effect of pH value of MO solution on MO adsorption.

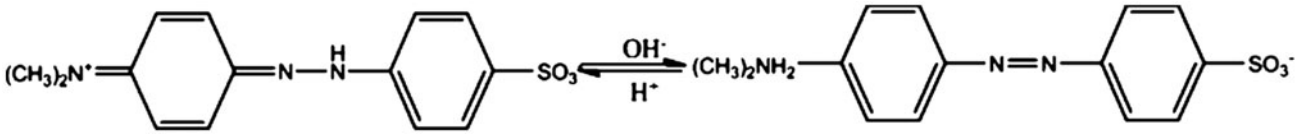

mainly positively charged, thus, a weak attraction between the positively charged composite and the negative functional groups of MO occurred, leading to low removal. With increase in pH from 3 to 7, a slight decrease in removal from 98.7 to 97.4% was observed. In this case, the MO existed in right pattern, the number of negatively charged sites in MO enhanced, while the surface of ECCS/BT composite was still positively charged, and partial $-NH_2$ groups in adsorbent were protonated into $-NH_3^+$ groups, so the electrostatic attraction between the negatively charged MO anions and the positively charged surface of the adsorbent enhanced, resulting in high removal. However, above pH 7, decreasing removal may be due to the competition of hydroxyl ions in the solution with the dye anions for adsorptive sites and the electrostatic repulsive force between the negatively charged surface and the anionic dye. Similar results from MO adsorption onto the multi-walled carbon nanotubes and activated carbons of corncob-derived char wastes were reported by Yao et al. [24] and Hou et al. [25].

3.5. Effect of adsorbent dosage on MO adsorption

The effect of adsorbent dosage on MO adsorption onto the ECCS/BT composite is shown in Fig. 8. An increase in adsorbent dosage from 0.2 to 1 g/L resulted in the increase in the removal from 31.2 to 92.7%. This increase in removal was due to the increase of adsorption active sites on the adsorbent surface when increasing adsorbent dosage. A further increase in adsorbent dosage beyond 1 g/L exhibited no extra improvement in dye removal. However, the adsorption capacity for MO decreased with increasing the adsorbent dosage (Fig. 8). This trend could be attributed to the unsaturation of adsorption sites, where there was a greater number of unoccupied binding sites of the ECCS/BT composite at higher dosages due to the equilibrium with each other between the surface and solution concentration of MO. Similar behavior has been observed for the removal of humic acid from aqueous solution by surfactant-modified chitosan/zeolite composites [26]. Therefore, considering the removal together with the

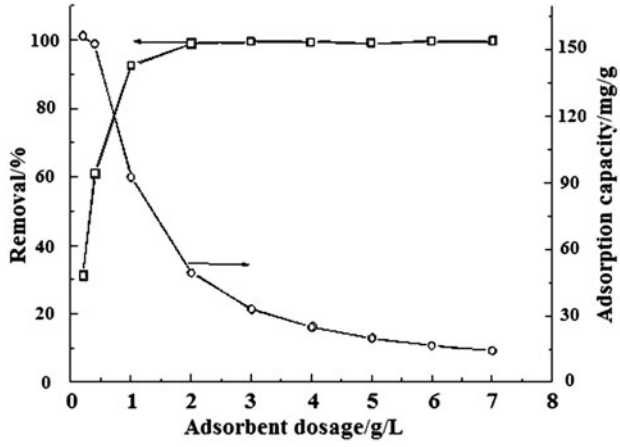

Fig. 8. Effect of adsorbent dosage on MO adsorption.

adsorption capacity, 1 g/L adsorbent dosage was chosen for later studies.

3.6. Effect of initial MO concentration on MO adsorption

Experiments were carried out at various MO concentrations while the other parameters were kept constant. As shown in Fig. 9, the adsorption capacity

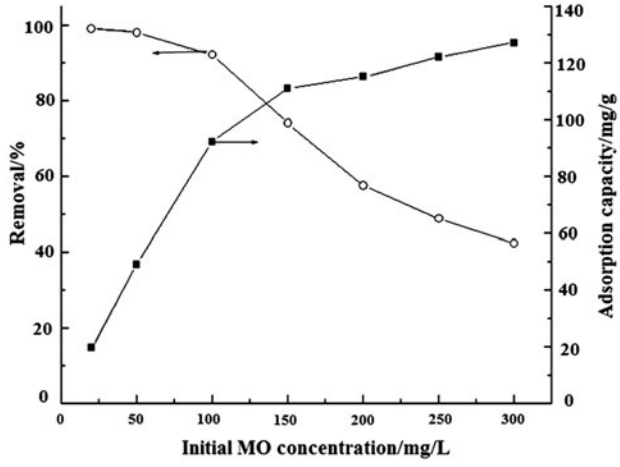

Fig. 9. Effect of initial MO concentration on MO adsorption.

improved with increasing dye concentrations. The high MO concentration can result in a high mass gradient pressure between the solution and adsorbent, which acted as a driving force to transfer dye molecules from bulk solution to the particle surface, and therefore to overcome the mass transfer resistance between the aqueous and solid phase. Thus, higher MO concentrations enhanced the adsorption capacity. Many researchers have reported the similar observations for MO adsorption by various adsorbents [10,23]. However, the removal showed an opposite trend. When the initial concentration increased from 20 to 300 mg/L, the removal decreased from 99.7 to 42.4%. This trend may be explained as follows: at lower concentrations, the ratio of initial number of MO to the available adsorption sites was low and subsequently more sites were available for MO adsorption, thus the removal increased. When MO concentrations were lower than 100 mg/L, the removal was higher than 92%. However, at higher concentrations, the ratio of initial number of the available adsorption sites to MO molecules was low; fewer sites were used for adsorption, so the removal was decreased.

3.7. Effect of contact time on MO adsorption

Equilibrium time is one of the most important parameters in the design of economical wastewater treatment systems. The adsorption of MO onto the ECCS/BT composite at various dye concentrations was studied as a function of contact time in order to determine the necessary adsorption equilibrium time. These results are shown in Fig. 10. The adsorption was rapid at the initial stages and then gradually decreased with increasing contact time until the equilibrium was attained. The rapid adsorption at the initial contact time can be attributed to the availability of large number of vacant sites for MO adsorption, and the slow rate of dye adsorption was probably due to the decreasing gradient pressure between the solution and adsorbent. Besides, longer equilibrium time was required with increasing initial MO concentrations, and the equilibrium time for MO solutions at 50, 100, and 150 mg/L was 20, 60, and 100 min, respectively. Similar result has been reported by Chen et al. for MO and methyl violet adsorption on activated carbon derived from phragmites australis [23]. For the sake of the attainment of equilibrium, 180 min was considered to be the optimum equilibrium time in further experiments.

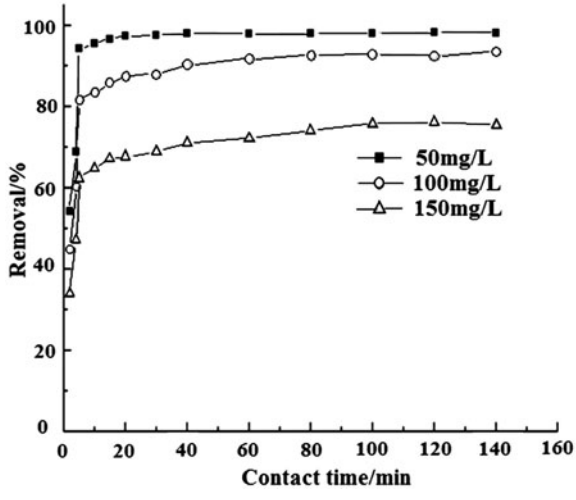

Fig. 10. Effect of contact time on MO adsorption.

3.8. Adsorption isotherms

In this study, two commonly used models, the Freundlich and Langmuir isotherms were applied to understand the interaction between the adsorbate and adsorbents. The Freundlich isotherm is an empirical equation assuming that the adsorption process takes place on a heterogeneous surface through a multilayer adsorption mechanism. The Freundlich isotherm is expressed by the following equation:

$$\log q_e = \log K_F + \frac{1}{n} \log C_e \tag{3}$$

where q_e (mg/g) is the amount of MO adsorbed per unit of adsorbent at equilibrium, C_e (mg/L) is the MO concentration at equilibrium, K_F ((mg/g)(L/mg)$^{1/n}$) and n are the Freundlich constants related to adsorption capacity and heterogeneity factor, respectively. The values of K_F and n can be calculated from the intercept and slope of the linear plot between log C_e and log q_e (Fig. 11).

The Langmuir adsorption model is based on the assumption that the adsorption process takes place on a specific homogeneous surface through a monolayer adsorption. The equation is given as follows:

$$\frac{C_e}{q_e} = \frac{1}{Qb} + \frac{C_e}{Q} \tag{4}$$

where C_e (mg/L) is the MO concentration at equilibrium, q_e (mg/g) is the amount of MO adsorbed per unit of adsorbent at equilibrium, Q (mg/g) is the maximum amount of adsorption with complete monolayer coverage on the adsorbent surface, and b (L/mg)

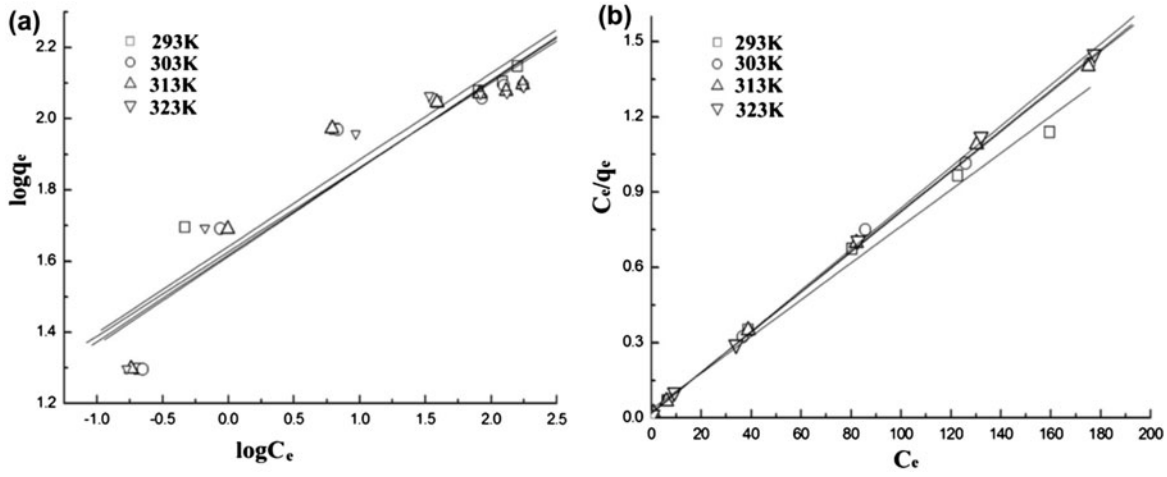

Fig. 11. Freundlich (a) and Langmuir(b) plots for the adsorption of MO onto enhanced cross-linked chitosan/bentonite composite at different temperatures.

is the Langmuir constant, which is related to the energy of adsorption. The Langmuir constants, b and Q, can be determined from the intercept and slope of the linear plot of C_e/q_e vs. C_e (Fig. 11).

The essential characteristics of the Langmuir isotherm can be expressed in terms of a dimensionless constant separation factor R_L [27], which is given by Eq. (5):

$$R_L = \frac{1}{1 + bC_0} \tag{5}$$

where C_0 (mg/L) is the initial MO concentration and b (L/mg) is the Langmuir constant. If the R_L value is between 0 and 1, the adsorption process is favorable.

All the correlation coefficients, R^2 values, and the constants obtained from the two isotherm models are summarized in Table 1. The Langmuir isotherm model gave the higher R^2 values which were greater than 0.99 at all temperatures studied as compared with the Freundlich model, indicating that the adsorption of MO on the ECCS/BT composite was best described by the Langmuir model, and it occurred as a monolayer coverage process. The values of R_L were found to be between 0 and 1, indicating that the adsorption of MO on the ECCS/BT composite was favorable. The adsorption capacity decreased with the increasing adsorption temperature, indicating that the adsorption of MO was favored at lower temperatures. Table 2 lists a comparison of the maximum adsorption capacity (Q_{max}) of MO on various adsorbents [10,22,28–31]. The ECCS/BT composite exhibited a relatively large adsorption capacity (136.8 mg/g), suggesting that it may be a low-cost and effective adsorbent for the removal of MO from aqueous solutions.

Table 1
Langmuir and Freundlich isotherm parameters of MO adsorption onto this composite

Isotherms	Parameters	293 K	303 K	313 K	323 K
Langmuir isotherm	Q	136.8	125.2	124.5	122.1
	b	0.2253	0.3692	0.3809	0.4820
	R_L	0.018–0.182	0.027–0.119	0.028–0.116	0.034–0.094
Freundlich isotherm	R^2	0.9961	0.9993	0.9995	0.9997
	K_F	43.74	40.94	41.38	42.23
	n	4.107	4.040	4.093	4.212
	R^2	0.9349	0.9362	0.9413	0.9440

Table 2
Comparison of the maximum monolayer adsorption capacities of MO on various adsorbents

Adsorbent	Adsorption capacity (mg/g)	Refs.
Acid-modified carbon-coated monolith	147.06	[10]
Chitosan/maghemite composite	779	[22]
Maghemite/chitosan films	29	[28]
Carbon-coated monolith	102.04	[29]
Chitosan/Al_2O_3/magnetite nanoparticles	417	[30]
Ammonium-functionalized silica nanoparticles	105.4	[31]
Enhanced cross-linked chitosan/bentonite composite	136.8	This study

3.9. Adsorption kinetics

In order to characterize the kinetics involved in the process of adsorption, the pseudo-first-order and pseudo-second-order kinetic models were proposed and used to fit the experimental data from the adsorption of MO onto the ECCS/BT composite. The pseudo-first-order kinetic model can be represented by the following equation [32]:

$$\log(q_e - q_t) = \log q_e - \frac{k_1}{2.303}t \quad (6)$$

where q_e (mg/g) and q_t (mg/g) are the amounts of adsorbate adsorbed at equilibrium and at contact time t (min), respectively, and k_1 (min^{-1}) is the pseudo-first-order rate constant. The values of q_e and k_1 for the pseudo-first-order kinetic model were determined from the intercept and the slope of the plot of log ($q_e - q_t$) vs. t (Fig. 12), respectively. The k_1 values, correlation coefficient values, and q_e values (experimental and calculated) are summarized in Table 3. The correlation coefficients, R^2 values for the pseudo-first-order model changed in the range of 0.9309–0.9522 for MO adsorption. Besides, the experimental q_e values, $q_{e,exp}$ did not agree with the calculated values, $q_{e,cal}$ obtained from the linear plots. It suggests that the adsorption of MO did not follow the pseudo-first-order kinetic model.

The pseudo-second-order kinetic model can be represented in the following form [33]:

$$\frac{t}{q_t} = \frac{1}{k_2 q_e^2} + \frac{1}{q_e}t \quad (7)$$

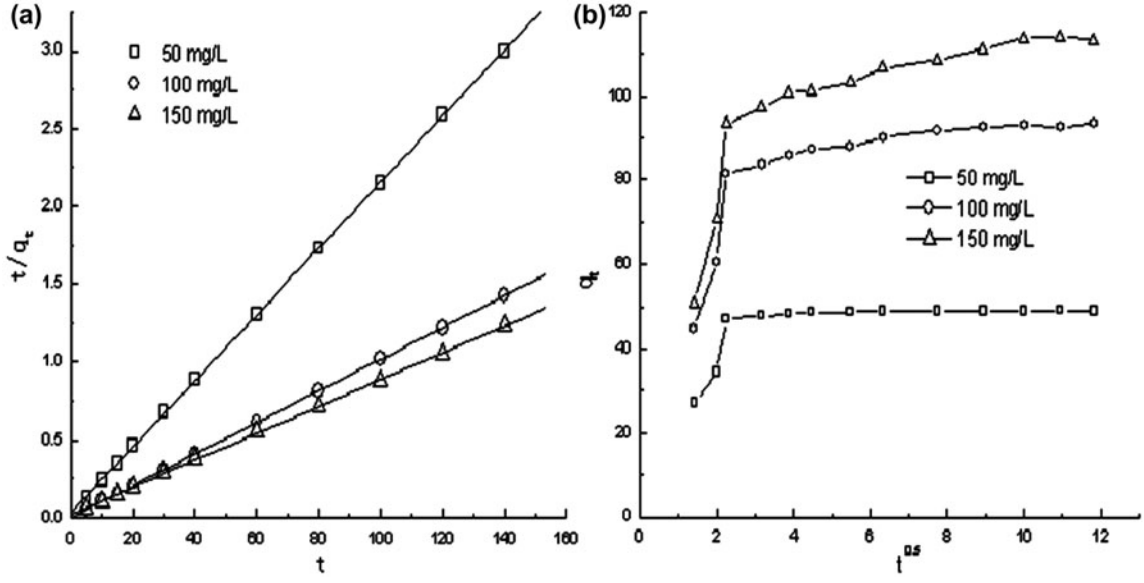

Fig. 12. Pseudo-second-order kinetics (a) and intraparticle diffusion (b) plots for the adsorption of MO onto enhanced cross-linked chitosan/bentonite composite at different concentrations.

Table 3
Pseudo-first-order and pseudo-second-order kinetic model parameters

Parameters	Pseudo-first-order kinetic model				Pseudo-second-order model		
	k_1	$q_{e,cal}$	R^2	$q_{e,exp}$	k_2	$q_{e,cal}$	R^2
50	0.0428	39.92	0.9522	46.67	0.0445	47.08	0.9998
100	0.0269	72.28	0.8673	97.89	0.0146	98.33	0.9999
150	0.0404	97.70	0.9309	114.1	0.0034	115.5	0.9998

where k_2 (g/(mg min)) is the rate constant of pseudo-second-order adsorption. The k_2 and q_e values determined from the slope and intercepts of the plot of t/q_t vs. t (Fig. 12) are presented in Table 3 along with the corresponding correlation coefficients. The correlation coefficients (R^2) values for the pseudo-second-order kinetic model were greater than 0.999 for all MO concentrations, indicating the applicability of the pseudo-second-order kinetic model to describe the adsorption process of MO on the ECCS/BT composite. The calculated q_e value according to the pseudo-second-order model agreed well with the experimental data at different initial MO concentrations. Therefore, the adsorption of MO was better described by the pseudo-second-order kinetic model rather than the pseudo-first-order kinetic model. Besides, the k_2 value decreased with increasing MO concentrations, thus, the adsorption equilibrium time for MO solution with higher concentration would be prolonged due to the lower k_2 values, which was in accordance with those results mentioned in Section 3.7.

3.10. Desorption and reusability studies

To investigate the reusability of the ECCS/BT composite, the adsorption–desorption–adsorption was conducted, and the results are shown in Table 4. It is shown that, on the contrary to NaOH solution, HCl was preferred solution for desorption and reusability studies of the ECCS/BT composite due to the relatively high RRs (>75%). So, it can be stated that the ECCS/BT composite can be renewed with HCl solution.

Table 4
Regeneration of ECCS/BT composite

Eluent reagent	Regeneration rate (%)
0.1 mol/L HCl	77.0
0.3 mol/L HCl	79.5
0.5 mol/L HCl	82.9
0.1 mol/L NaOH	61.7
0.3 mol/L NaOH	49.4
0.5 mol/L NaOH	41.1

4. Conclusion

ECCS/BT composite is identified to be a low-cost and effective adsorbent for the removal of MO from aqueous solutions. MO was found to be adsorbed strongly by the ECCS/BT composite due to the activation of bentonite and the protonation of $-NH_2$ groups in chitosan. The maximum removal occurred at pH 3. The removal increased with an increase in adsorbent dosage and contact time while it decreased with increasing dye concentration. The equilibrium time for MO adsorption was prolonged with increasing initial MO concentrations. The equilibrium data were best described by the Langmuir isotherm model, and the maximum monolayer adsorption capacity was obtained at 136.8 mg/g at natural pH and 293 K. The adsorption kinetic data can be described by the pseudo-second-order kinetic model.

Acknowledgment

This work was supported by the National Natural Science Foundation of China (grant number 51003086).

References

[1] A.E. Ofomaja, Y.S. Ho, Effect of temperatures and pH on methyl violet biosorption by Mansonia wood sawdust, Bioresour. Technol. 99 (2008) 5411–5417.
[2] K. Kadirvelu, M. Kavipriya, C. Karthika, M. Radhika, N. Vennilamani, S. Pattabhi, Utilization of various agricultural wastes for activated carbon preparation and application for the removal of dyes and metal ions from aqueous solutions, Bioresour. Technol. 87 (2003) 129–132.
[3] Y. Wang, M. Yao, Y. Chen, Y. Zuo, X. Zhang, L. Cui, General synthesis of magnetic mesoporous FeNi/graphitic carbon nanocomposites and their application for dye adsorption, J. Alloys Compd. 627 (2015) 7–12.
[4] J. Mittal, D. Jhare, H. Vardhan, A. Mittal, Utilization of bottom ash as a low-cost sorbent for the removal and recovery of a toxic halogen containing dye eosin yellow, Desalin. Water Treat. 52(22–24) (2014) 4508–4519.
[5] J. Mittal, V. Thakur, A. Mittal, Batch removal of hazardous azo dye Bismark Brown R using waste material hen feather, Ecol. Eng. 60 (2013) 249–253.

[6] G. Sharma, M. Naushad, D. Pathania, A. Mittal, G.E. El-desoky, Modification of *Hibiscus cannabinus* fiber by graft copolymerization: Application for dye removal, Desalin. Water. Treat. 54(11) (2014) 1–8, doi:10.1080/19443994.2014.904822.
[7] R. Elmoubarki, F.Z. Mahjoubi, H. Tounsadi, J. Moustadraf, M. Abdennouri, A. Zouhri, A. El Albani, N. Barka, Adsorption of textile dyes on raw and decanted Moroccan clays: Kinetics, equilibrium and thermodynamics, Water Resour. Ind. 9 (2015) 16–29.
[8] T. Yao, S. Guo, C. Zeng, C. Wang, L. Zhang, Investigation on efficient adsorption of cationic dyes on porous magnetic polyacrylamide microspheres, J. Hazard. Mater. 292 (2015) 90–97.
[9] K.N. Aboua, Y.A. Yobouet, K.B. Yao, D.L. Goné, A. Trokourey, Investigation of dye adsorption onto activated carbon from the shells of Macoré fruit, J. Environ. Manage. 156 (2015) 10–14.
[10] W. Cheah, S. Hosseini, M. Khan, T.G. Chuah, T.S.Y. Choong, Acid modified carbon coated monolith for methyl orange adsorption, Chem. Eng. J. 215–216 (2013) 747–754.
[11] M.V. Dinu, E.S. Dragan, Evaluation of Cu^{2+}, Co^{2+} and Ni^{2+} ions removal from aqueous solution using a novel chitosan/clinoptilolite composite: Kinetics and isotherms, Chem. Eng. J. 160 (2010) 157–163.
[12] M. Auta, B.H. Hameed, Chitosan–clay composite as highly effective and low-cost adsorbent for batch and fixed-bed adsorption of methylene blue, Chem. Eng. J .237(2014)352–361.
[13] L. Zeng, M. Xie, Q. Zhang, Y. Kang, X. Guo, H. Xiao, Y. Peng, J. Luo, Chitosan/organic rectorite composite for the magnetic uptake of methylene blue and methyl orange, Carbohydr. Polym. 123 (2015) 89–98.
[14] D.W. Cho, B.H. Jeon, C.M. Chon, Y. Kim, F.W. Schwartz, E.S. Lee, H. Song, A novel chitosan/clay/magnetite composite for adsorption of Cu (II) and As(V), Chem. Eng. J. 200–202 (2012) 654–662.
[15] F.A.R. Pereira, K.S. Sousa, G.R.S. Cavalcanti, M.G. Fonseca, A.G. de Souza, A.P.M. Alves, Chitosan-montmorillonite biocomposite as an adsorbent for copper(II) cations from aqueous solutions, Int. J. Biol. Macromol. 61 (2013) 471–478.
[16] R. Huang, Q. Liu, L. Zhang, B. Yang, Utilization of cross-linked chitosan/bentonite composite in the removal of methyl orange from aqueous solution, Water. Sci. Technol. 71 (2015) 174–182.
[17] L. Zhang, X. Liu, W. Xia, W. Zhang, Preparation and characterization of chitosan-zirconium(IV) composite for adsorption of vanadium(V), Int. J. Biol. Macromol. 64 (2014) 155–161.
[18] A.A. Jalil, S. Triwahyono, M.R. Yaakob, Z.Z. Azmi, N. Sapawe, N.H.N. Kamarudin, H.D. Setiabudi, N.F. Jaafar, S.M. Sidik, S.H. Adam, B.H. Hameed, Utilization of bivalve shell-treated Zea mays L. (maize) husk leaf as a low-cost biosorbent for enhanced adsorption of malachite green, Bioresour. Technol. 120 (2012) 218–224.
[19] W. Ma, X. Song, Y. Pan, Z. Cheng, G. Xin, B. Wang, X. Wang, Adsorption behavior of crystal violet onto opal and reuse feasibility of opal-dye sludge for binding heavy metals from aqueous solutions, Chem. Eng. J. 193–194 (2012) 381–390.
[20] E.N. El Qada, S.J. Allen, G.M. Walker, Adsorption of Methylene Blue onto activated carbon produced from steam activated bituminous coal: A study of equilibrium adsorption isotherm, Chem. Eng. J. 124 (2006) 103–110.
[21] N. Viswanathan, C.S. Sundaram, S. Meenakshi, Removal of fluoride from aqueous solution using protonated chitosan beads, J. Hazard. Mater. 161 (2009) 423–430.
[22] L. Obeid, A. Bée, D. Talbot, S. Jaafar, V. Dupuis, S. Abramson, V. Cabuil, M. Welschbillig, Chitosan/maghemite composite: A magsorbent for the adsorption of methyl orange, J. Colloid Interface Sci. 410 (2013) 52–58.
[23] S. Chen, J. Zhang, C. Zhang, Q. Yue, Y. Li, C. Li, Equilibrium and kinetic studies of methyl orange and methyl violet adsorption on activated carbon derived from Phragmites australis, Desalination 252 (2010) 149–156.
[24] Y. Yao, B. He, F. Xu, X. Chen, Equilibrium and kinetic studies of methyl orange adsorption on multiwalled carbon nanotubes, Chem. Eng. J. 170 (2011) 82–89.
[25] X. Hou, Q. Deng, T. Ren, Z. Yuan, Adsorption of Cu^{2+} and methyl orange from aqueous solutions by activated carbons of corncob-derived char wastes, Environ. Sci. Pollut. Res. 20 (2013) 8521–8534.
[26] J. Lin, Y. Zhan, Adsorption of humic acid from aqueous solution onto unmodified and surfactant-modified chitosan/zeolite composites, Chem. Eng. J. 200–202 (2012) 202–213.
[27] K.R. Hall, L.C. Eagleton, A. Acrivos, T. Vermeulen, Pore- and solid-diffusion kinetics in fixed-bed adsorption under constant-pattern conditions, Ind. Eng. Chem. Fundam. 5 (1966) 212–223.
[28] R. Jiang, Y. Fu, H. Zhu, J. Yao, L. Xiao, Removal of methyl orange from aqueous solutions by magnetic maghemite/chitosan nanocomposite films: Adsorption kinetics and equilibrium, J. Appl. Polym. Sci. 125 (2012) E540–E549.
[29] S. Hosseini, M.A. Khan, M.R. Malekbala, W. Cheah, T.S.Y. Choong, Carbon coated monolith, a mesoporous material for the removal of methyl orange from aqueous phase: Adsorption and desorption studies, Chem. Eng. J. 171 (2011) 1124–1131.
[30] B. Tanhaei, A. Ayati, M. Lahtinen, M. Sillanpää, Preparation and characterization of a novel chitosan/Al_2O_3/magnetite nanoparticles composite adsorbent for kinetic, thermodynamic and isotherm studies of Methyl Orange adsorption, Chem. Eng. J. 259 (2015) 1–10.
[31] J. Liu, S. Ma, L. Zang, Preparation and characterization of ammonium-functionalized silica nanoparticle as a new adsorbent to remove methyl orange from aqueous solution, Appl. Surf. Sci. 265 (2013) 393–398.
[32] H. Zhu, R. Jiang, L. Xiao, G.M. Zeng, Preparation, characterization, adsorption kinetics and thermodynamics of novel magnetic chitosan enwrapping nanosized γ-Fe_2O_3 and multi-walled carbon nanotubes with enhanced adsorption properties for methyl orange, Bioresour. Technol. 101 (2010) 5063–5069.
[33] C.H. Wu, Adsorption of reactive dye onto carbon nanotubes: Equilibrium, kinetics and thermodynamics, J. Hazard. Mater. 144 (2007) 93–100.